INVESTIGATIONS OF DELAMINATION GROWTH RATES AND CRITICALITY ALONG HETEROGENEOUS INTERFACES

J.C. Thesken, F. Brandt and S. Nilsson
The Aeronautical Research Institute of Sweden (FFA)
P.O. Box 11021, S-161 11 Bromma, Sweden

Abstract

Progress is reported for an ongoing investigation of delamination growth along 0°/0°, 0°/5°, ±5°, and 0°/90° interfaces in carbon fiber /epoxy composites. The work aims to determine relationships between damage criticality, growth rate and acoustic emission activity for delamination along heterogeneous interfaces. The final objective is to asses the transferability of such relationships between laboratory coupons and composite structural elements.

A family of delamination specimens containing one or a few off-axis plies sandwiched between bulk layers of 0° material is tested. Two types of sandwhich laboratory coupons, conventional delamination beams and rigidly loaded single edge notched strips, are compared for different mode ratios. Buckling induced delamination plates represent composite structural elements; an example is reviewed. The application of a graphite crack gauge to measure delamination length and growth rate in carbon fiber composites is described. Delamination growth rates ranging from $5 \cdot 10^{-5}$ m/s to 2000 m/s are recorded. Visual, C-scan, X-ray, macro-video and acoustic emission measurements are used to follow damage evolution.

Empirical evaluations of delamination criticality are made for delamination beams using the Irwin-Kies relation. Interface effects and through thickness constraint for sandwich coupons are analyzed using a three dimensional p-version of the finite element method. The results indicated that the single edge notch strip could be analyzed as a two dimensional homogeneous body. Unstable growth is analyzed using two dimensional elasto-dynamic moving finite elements. The analysis of buckling induced delamination is made using plate/shell finite element methods together with growth/remeshing algorithms.

Copyright © 1994 by ICAS and AIAA. All rights reserved.

Introduction

Background

The work described here is an overview of the FFA contribution to the Group for Aeronautical Research and Technology in Europe's Action Group 16 *Damage Propagation in Composite Structural Elements*.[1] The purpose for the formation of the group is to improve the modelling and prediction of composite structural performance in the presence of impact damage or manufacturing defects. The precise program objectives are as follows:

- Improve the understanding of delamination growth onset by careful experimentation including NDE and fractography.
- Check the validity range of current delamination growth models by analysis and prediction of residual strength.
- Identify correspondence and basic differences between damage growth in coupons and in structural elements.
- Identify the current potential for improvement of design procedures.

These objectives run in parallel with FFA's own efforts to develop health monitoring systems and damage evaluation procedures for full scale composite aircraft components. Acoustic emission is one of the passive NDT methods being explored in this respect and its use as a predictor of delamination growth and criticality shall be discussed in a companion paper.[2] The necessary experimental and theoretical investigations of delamination growth are reviewed here. The specific goals are 1.) to determine the relationship between damage criticality, growth rate and acoustic emission activity of a delamination extending along realistic interfaces, and 2.) to examine the transferability of such relationships from laboratory specimen geometries to geometries representative of composite structural elements.

Program Scope

Of the many damage processes occurring in continuous fiber reinforced composites , delamination growth is often the largest in terms of characteristic

dimensions. Therefore the size of a delamination and its growth rate strongly influences the degradation of residual strength in composite structures. This accounts for the motivation to apply fracture mechanics to predict the initiation and growth of damage in composite structures.[3,4] However, looking at finer length scales reveals that fiber failure, matrix fracture and fiber/matrix separation are all likely participants in such damage growth. These complex features certainly influence the system of loads controlling the extension of the delamination front and the governance of damage growth methodologies.

Sandwich specimen. Conventional delamination testing has generated much data for homogenous unidirectional lay-ups but these results do not accurately represent real damage growth along heterogeneous interfaces. Certainly this situation is likely to carry over to the nature of acoustic emission signatures for different interfaces. A means to obtain heterogeneity along a representative delamination interface is therefore central to this work. Here it is proposed that a sandwich of one or a few off-axis plies between bulk layers of 0° material will trap a delamination and its attending damage mechanisms to create an isolated interface system (see fig. 1). The interfaces treated thus far include: 0°/0°, 0°/5°, ±5° and 0°/90°. All laminates were made with the toughened epoxy prepreg HTA/6376C from Ciba-Giegy.

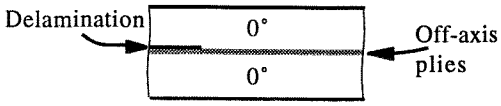

Fig. 1 Laminate sandwhich specimen.

Fiber orientation effects on delamination have been examined experimentally by several authors, a review is given in ref.[5] The interfaces treated here are at far ends of a spectrum of behaviour. The 0°/5° and ±5° are intended to prevent fiber bridging as in the small angle interface experiments by Johnson and Magalgiri[6] The 0°/90° interface is similar to the cross-ply interface studied by Wilkens et al[7] where intralaminar growth in the 90° ply was observed.

The development of interface toughness criteria is hindered by well known difficulties concerning mode coupling and complex singularities. A complete specification of interface toughness requires experiments which span the ratio of coupled modes.[8] The use here of sandwich specimens may simplify this procedure as demonstrated by Suo and Hutchinson[9] for isotropic sandwiches. Their results infer whether the stress intensity factors for a homogenous body could be used as a good approximation of the actual (complex) interface stress intensity factors. This analysis has yet to be extended to orthotropic materials; however, Hutchinson[10] notes that the "orthotropic rescaling" procedure presented by Suo et al[11] could be used to generalize these results.

The application of such an analysis relies on the equivalency of the global G for the homogenous body to the local G for the interface system. This equivalency is met so long as the sandwich layer is small with respect to other dimensions of the problem. As a first step to check this assumption, three dimensional finite element evaluations of the G distributions for the homogenous unidirectional problem shall be compared to the G distributions for the sandwich interfaces.

Further work is required to establish the interface toughness with respect to the ratio of the local coupled modes; however, there may be reasons not to carry the elastic analysis this far. Recall that the validity of any such criticality parameter is determined by the autonomy of the process zone. In cases where matrix yielding, microcracking and fiber bridging zones are the size of the sandwiched layer or greater, linear elastic fracture mechanics LEFM and related Irwin-Kies calibration methods become invalid. Large scale bridging analyses, such as those discussed by Suo et al[12], Bao and Suo[13], Östlund and Nilsson[14,15], are then required to determine residual strength. For now the roles of oscillatory interface stress singularities and large scale process zones are played down with caution. Results are presented in terms of G for a homogenous body where

$$G = G_{\mathrm{I}} + G_{\mathrm{II}} + G_{\mathrm{III}} \qquad (1)$$

and the subscripts I, II, III correspond to the separable loading modes.

Specimen configuration. A summary of the program line and the experimental configurations are illustrated in fig. 2. Two types of laboratory coupons shall be tested and compared: the conventional delamination beam and the single edge notched strip. These two configurations provide an opportunity to compare delamination criticality for a range of growth rates and growth stability behaviours. The delamination beams are being tested in double-cantilever beam (DCB), edge notch flexure (ENF), and mixed mode bending (MMB) configurations. The MMB testing is based on the rig developed by Crews and Reeder[16,17]. The single edge notched strips[18,19] are bonded to steel tabs and loaded in displacement control analogous to the infinite strip problems treated by Rice[20] and Nilsson[21]. Buckling induced delamination (BID) plates are proposed as representative composite structural elements. The program extends the approach presented by Nilsson et al[22] to more realistic configurations.

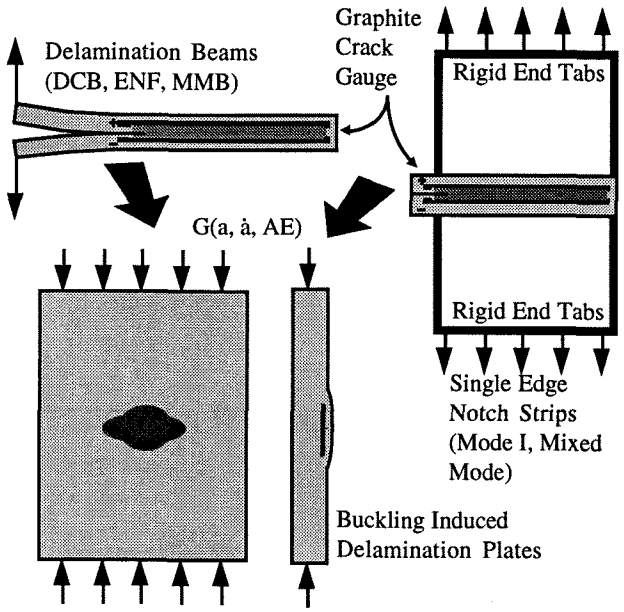

Fig. 2 Program line and experimental configurations.

Growth rate and Crack gauge. As indicated by the arrows in fig. 2, the program shall examine the transferability of delamination criticality data, for example G, from coupon specimen to structural elements. Related parameters in the study include crack length a, growth rate $\dot{a}$ and various measures of acoustic emission activity.

Growth rate is not a frequently measured parameter in delamination testing despite that rate effects are known to play an important role in interlaminar fracture.[23] Davies and Benzegagh[24] point out that the comparison of interlaminar toughness values for different specimens requires the definition of a true rate parameter. A common parameter for such characterization is the displacement rate just behind the crack tip.[23,25] However, Daniel and co-workers[26,27] have demonstrated that growth rate measurement is an interesting alternative rate parameter. Following their example, delamination velocity is studied here as a basis for developing growth prediction methods for both stable and unstable delamination extension.

The coupling of delamination criticality to acoustic emission also relies on growth rate measurements. Achenbach and Harris[28] have described a theoretical basis for the relationship of crack velocity to acoustic emission activity. Measurements made here are used in [2] to see if delamination growth rate and stability correlates with any observable AE phenomenon.

Thus an important development for the delamination coupon testing is the application of a resistive graphite film for crack length and growth rate measurements in carbon composites.[18,29] This graphite crack gauge is well known in polymer fracture testing; Stalder et al[30] provide a thorough development and critical analysis of the gauge for such application. Thesken[29] has examined the peculiarities and problems of gauge design and application for delamination measurements in carbon fiber composites. The gauge function and its performance during delamination testing are reviewed.

Analysis Methods. Where possible empirical evaluations of load, displacement and crack length are used to develop Irwin-Kies based delamination resistance curves. In particular, fully instrumented MMB tests have been made and a mode separation method is demonstrated which relies entirely on experimental measurements.

The numerical analysis thus far have focused on three dimensional studies of the sandwich specimen for 0°/0°, 0°/5° and ±5° interface systems. STRIPE, a p-version of the finite element method having edge and vertex intensity factor extraction methods is used for this purpose.[31,32] The initial goal is to see if 3-d analysis of the sandwich could be replaced by 2-d analysis of the homogenous specimen.

The single edge notch strip specimens have been modelled using 2-d finite element methods and G is determined using contour-area integral methods. Unstable fracture events are studied using the explicit elasto-dynamic code DYNCRACK which has the G-integral embedded in convecting crack tip elements.[33,18,19] The analysis of buckling induced delamination is made using plate/shell finite element methods and a growth/remeshing algorithms.[22,34]

Where appropriate fractography, ultrasonic C-scan and radiography are employed to follow the damage evolution processes. These results are discussed with respect to delamination growth rate and criticality data thus far computed.

Continuous Crack Growth Monitoring

Crack length and its rate of change with respect to other test parameters are essential measurements in any fracture toughness methodology. During slow stable growth, visual/optical methods are usually an adequate way of performing such measurements. However, rapid crack extensions of several millimeters may be observed in delamination experiments with continuous carbon fiber reinforced polymers. Indeed the unstable delamination growth observed for the rigidly extended strips often exceeded 1000 m/s.[18,19] Therefore the acquisition of crack length data must take place at an appropriate sampling rate.

The gauge used here consists of a thin graphite film in the shape of a narrow rectangular band ahead of the prospective crack path. The film may be applied directly to the specimen, if it is a non-conducting material. As shown in fig. 3a., voltage is applied through silver electrodes spaced a length b apart, along

each side of the band. The electrodes run parallel to the crack path and extend the length L_g of the gauge.

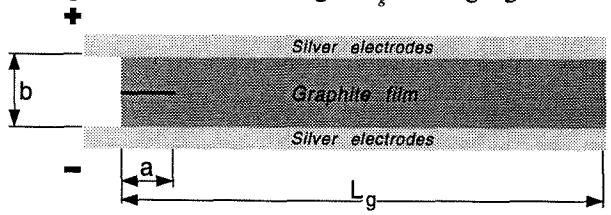

Fig. 3a Graphite crack gauge geometry.

Stalder et al[30] proposed a simple linear relation between changing gauge resistance R and crack length a as the crack separates the film:

$$\frac{R_o}{R} = 1 - \frac{a}{L_g} \qquad (2)$$

where R_o is the resistance of the initial uncracked film and a is the cracked length of the gauge.

The accuracy of this relation was checked empirically in [30] and fig. 3b describes the reported trends with respect to the line representing (2).

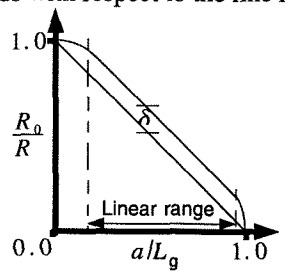

Fig. 3b Observed nonlinear behavior with respect to linear model, eqn. (2),[30] further verified.[29,37]

Depending on the aspect ratio b/L_g of the gauge, non-linear behaviour was observed for the beginning and end of the gauge. Therefore care must be taken in designing and positioning the gauge so that growth in the non-linear region is avoided. Also an empirically determined factor $\delta \approx 0.2(b/L_g)$ must be added to correctly evaluate the gauge in the linear region.[30]

Graphite Crack Gauge for Carbon Composites

Two technical problems arise when applying the graphite crack gauge to delamination growth measurements in carbon fiber composites. The first is the requirement to insulate the conductive film from the underlying carbon fibers. Here care must be taken so that the insulation behaves mechanically similar to the host material. The second problem is the limited space available on the narrow profile of common delamination specimens. This problem places design constraints on the gauge dimensions, electrode resistance, initial film resistance and also introduces manufacturing difficulties.

The peculiarities of gauge design and application for delamination measurements in carbon fiber composites have been discussed by Thesken[29]. Several insulation and gauge construction methods were evaluated before coming to the solution shown in fig. 4a. The method benefits from the bonding of a 25 μm thick Kapton™ film to the specimen profile using a strain gauge adhesive. This serves to insulate most of the specimen profile and reduce the possibility for electrical leakage. A window about 0.5 -0.7 mm is then precision cut along the prospective delamination growth path. This removes the mechanical influence of the Kapton™ film from the delamination process. Additional layers of strain gauge epoxy are then applied to the window to secure the insulation of the fracture process zone. Here the presence of the Kapton™ films on each side of the fracture plane guides the thickness of the epoxy insulation layer within the window.

After the insulation is completed, stencil techniques are used to apply silver electrodes and the graphite film.

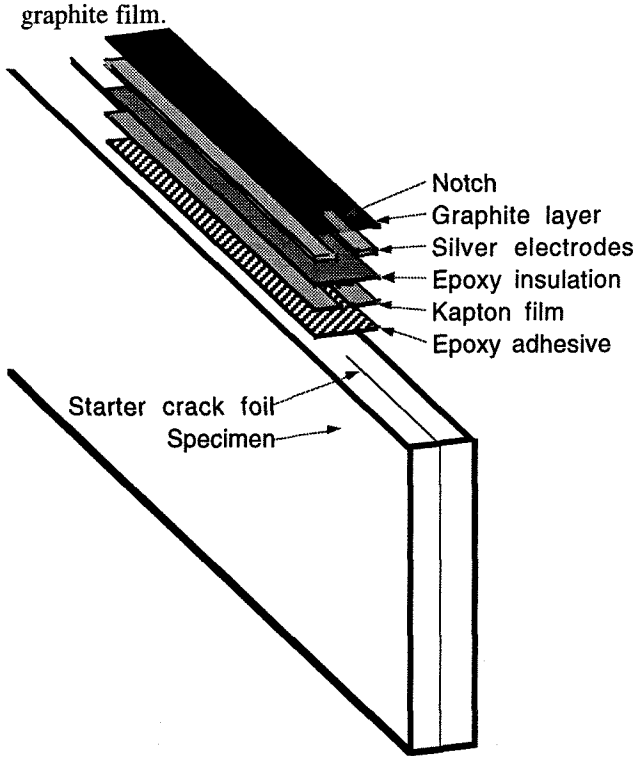

Fig.4a Graphite crack gauge construction.

Gauge dimensions in the following studies were kept so that $b/L_g \leq 0.1$. For such gauges, results in [30] indicates that ±1% accuracy is achievable in the linear range $0.4\,b/L_g < a/L_g < 0.95$. Figure 4b is an example of a finished gauge applied to a 3.0 mm DCB profile. Note that a starter crack has been masked so that delamination growth will begin within the linear range of the gauge.

The graphite crack gauges used in the following experiments usually had an initial resistance of 100 to

300 ohm. Electrode resistance was kept to less than 1% of the initial gauge resistance.

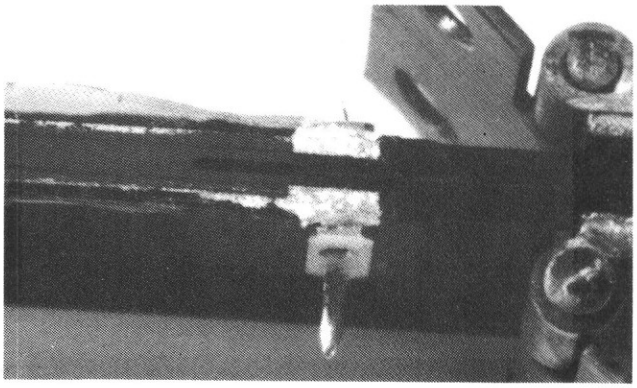

Fig. 4b DCB profile with crack gauge.

Measurement Circuit

The measurement circuit used here consisted of a simple shunt circuit shown in fig. 4c. A 1 to 10 ohm potentiometer was used as an adjustable shunt resistor and a 4.5 volt battery pack (V_b) was used as a noiseless voltage source.

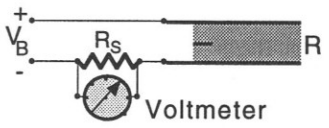

Fig. 4c Measurement circuit.

The voltage V across the shunt resistor can be related to crack length by:

$$a = L_g\left[(1+\delta) - \frac{(V_b/V_o)-1}{(V_b/V)-1}\right] \qquad (3)$$

V_o corresponds to the voltage in the initial uncracked gauge.[29] If the gauge is initially notched as in fig. 4b this value must be computed as part of the calibration procedure.[29]

Verification of the Gauge

The graphite crack gauge has been evaluated in comparison to measurements made visually, with the travelling microscope and from radiographs taken during DCB testing.[29] The corresponding voltage value is plotted for each type of crack length measurement in fig. 5 . The solid line is the conversion of voltage data from the crack gauge to crack length using (3). The excellent agreement between the travelling microscope and radiographic measurements has encouraged further use of the graphite crack gauge in delamination testing.

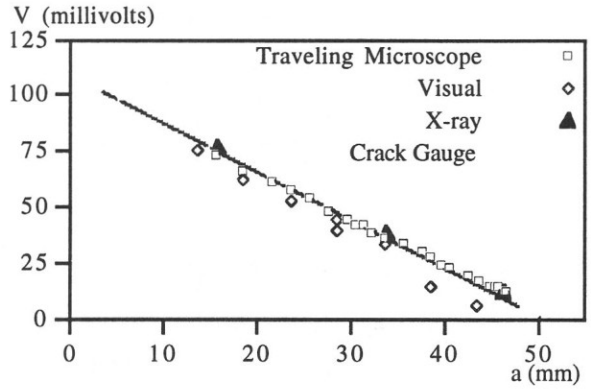

Fig. 5 Verification of graphite crack gauge performance for DCB testing.

Delamination Beam Specimens

Lay-up and specimen preparation

The 0°/0°, 0°/5° and 0°/90° interfaces for the delamination beam specimens were created from the following respective lay-ups: $0°_{24}$, $(0°_{12}/\pm5°/0°_8/\pm5°)$, and $(0°_{12}/90°/0°_{12})$. The starter crack was inserted after the 12th unidirectional layer in all cases. The majority of starter cracks were initiated from 13 μm thick Al-foil insert coated with Teflon™. However the test matrix also included the investigation of a Teflon™ paint starter crack for a few of the 0°/5° interfaces. This was done to evaluate the influence of starter crack insert thickness. Ljung[35] reports that a 3 μm starter crack thickness is possible with only five layers of spray.

After curing the laminates were C-scanned for flaws and sectioned. The nominal specimen dimensions were:

width	20 mm	
thickness	3 mm	(24 plies)
length	≥145 mm	
initial crack length	25 mm	

After sectioning, specimens were insulated according to procedures outlined above. Hinges were then applied before the graphite crack gauge was stencilled into place.

Double Cantilever Beam

The DCB testing follows standard procedures outlined by Carlsson and Pipes.[36] Further details are available in the student thesis by Brandt and Frii.[37] A photograph of the experimental set-up is shown in fig. 6. Displacements are measured by a wheel potentiometer drawn by a wire attached to the specimen. Loads, displacements and the crack gauge voltage are acquire by a Macintosh PC equipped with WorkBench™ software.

Travelling microscope measurements and a macro-ccd camera/video recorder were also used to follow growth.

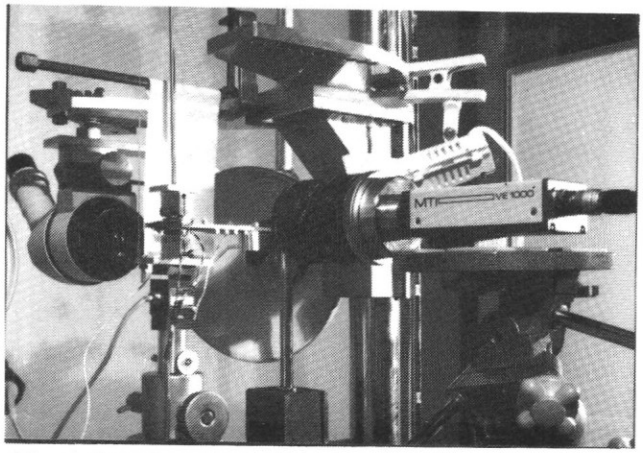

Fig. 6 DCB test set-up showing traveling microscope and macro-ccd camera.

Data Reduction and Analysis. Figure 7 presents examples of the load (P) vs displacement (d) data for the three types of interfaces tested plus the 0°/5° spray interface.

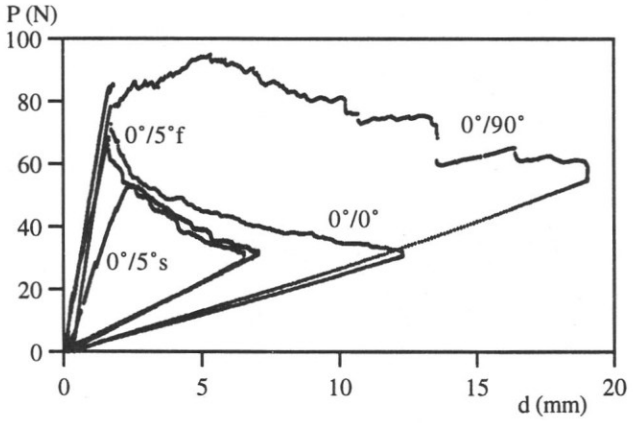

Fig. 7 Representative load vs. diaplacement curves for all interfaces.

For most cases the displacement was observed to return to zero when the specimen is unloaded. This means that the load, displacement and continuous crack length data can be used to generate continuous delamination resistance curves in a simple procedure.[29] First specimen compliance C is evaluated as

$$C = \frac{d}{P} \tag{4}$$

from the load and displacement data and plotted against a. The derivative dC/da is then determined from a curve fit. The energy release rate G can then be evaluated as a function of crack length using the Irwin-Kies formula.

$$G = \frac{P^2}{2w}\frac{dC}{da} \tag{5}$$

w is specimen width.

Experimental data for a 0°/0° interface is used to illustrate this point in fig. 8. A continuous crack length a vs d curve is shown in fig. 8a and the corresponding C vs a curve shown in fig. 8b.

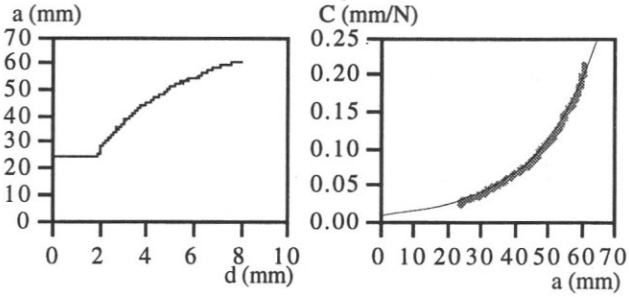

Fig. 8 Example energy release rate data reduction. a) Crack length vs displacement data. b) Compliance vs crack length plot with curve fit to determine dC/da.

A numerically computed curve fit to the data is also shown in fig. 8b. Several different types of curve fits have been examined in the study including: polynomial, logarithmic, exponential and power law. The choice of curve fit was made to give the best result in the initiation and early growth region of the data. Figure 8c shows an example of the resulting delamination toughness curve.

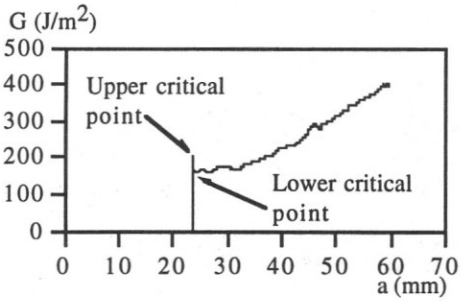

8c Continuous delamination toughness curve showing upper and lower critical points.

Figure 8c shows an upper and lower critical point which is associated with blunt starter cracks and the resin zone that occurs in front of thick inserts. This was a characteristic of the Al-foil for the 0°/0° and 0°/5° interfaces. The results for all three interface cases are summarized in fig. 9.

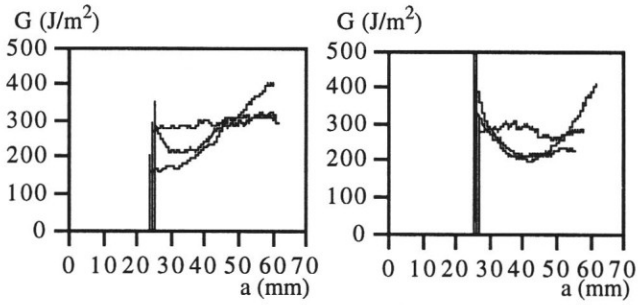

a) 0°/0° interface. b) 0°/5° interface.

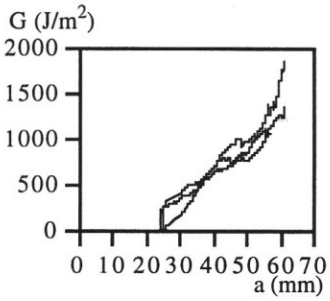

c) 0°/90° interface.

Fig. 9 Summary of delamination toughness curves.

Macro-fractography and Radiography. Images from the macro-ccd camera were recorded on video tape and later processed in an image analysis program.[37] The results show very clear differences in the respective fiber bridging processes. Three examples for each interface are shown in fig. 10. As expected, fiber intermingling along the 0°/0° interface produces large scale bridging zone in fig. 10a. However, in fig. 10b the population of bridging fibers is extremely reduced and the length of the zone shortened for the 0°/5°° interface. The 0°/90° interface in fig. 10c is clearly not an interlaminar fracture as the crack front winds its way through the 90° fibers releasing bundles of bridging fibers which lie parallel to the crack front. Here the bridging zone is nearly as long as the newly grown crack.

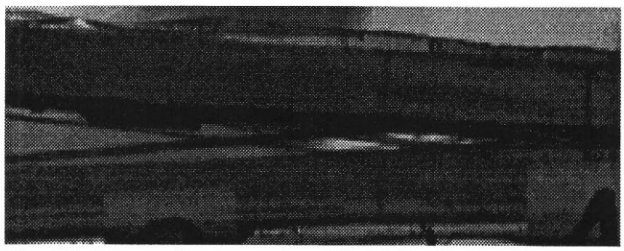

Fig. 10 Macro-fractography of bridging behavoir. a) 0°/0° interface.

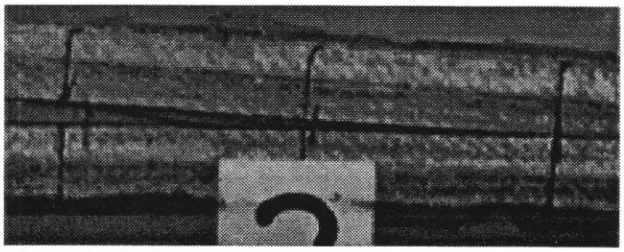

Fig. 10b 0°/5° interface.

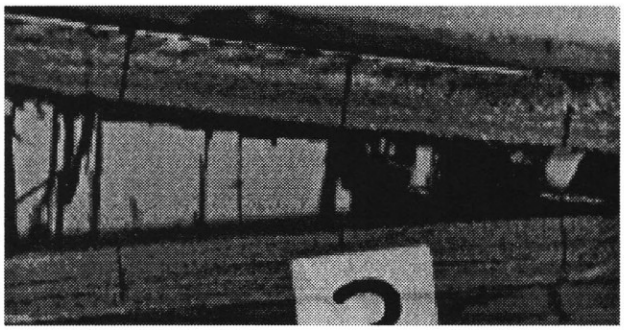

Fig. 10c 0°/90° interface.

Radiographs of the three interfaces appear in fig. 11. The crack front curvature of the 0°/0° and 0°/5° interfaces show the familiar concave shape reported in earlier DCB studies,[38] however, the X-ray photo for the 0°/90° interface shows a convex curve front.

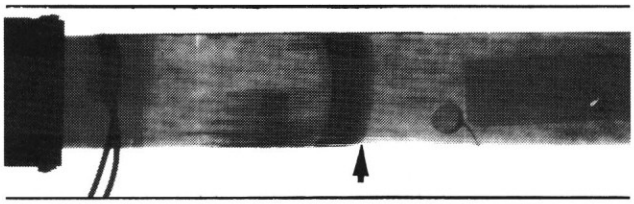

Fig. 11 Radiographs of crack front. a) 0°/0° interface.

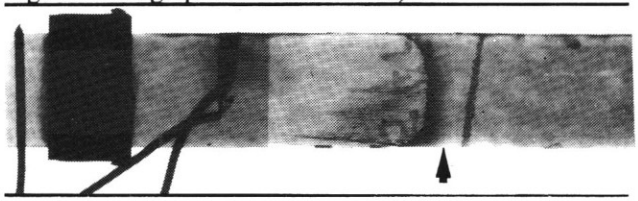

Fig. 11b 0°/5° interface.

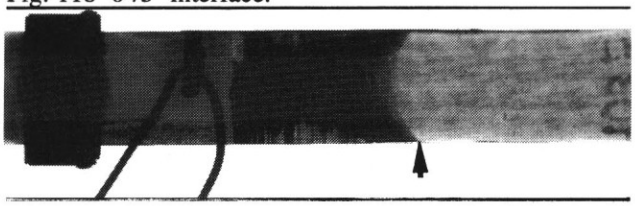

Fig. 11c 0°/90° interface.

Mixed Mode Bending

The mixed-mode testing was made with a modified version of the Crews and Reeder[16,17] mixed mode bending rig shown in fig. 12a. The rig used in these tests was originally constructed and tested by Ljung[35] using uni-directional beams of HTA/6376C. Several mixed-mode ratios for this material were examined, fig. 12b reports the interlaminar fracture toughness vs percentage G_{II}.

The following work seeks to extend this evaluation in two ways: 1) to fully determine the kinematic motion of the loading lever and its components during a mixed mode test. 2) to use empirical measurements to fully determine the mixed mode ratio during testing. The first of these objectives

was achieved by measuring two vertical displacements and one horizontal displacement during each experiment.

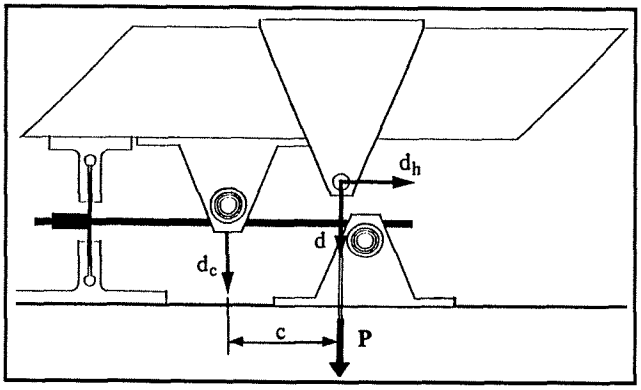

Fig. 12a FFA version of the MMB rig.[35]

As shown in fig. 12a, horizontal and vertical displacements are measured at the applied loading point and a horizontal displacement is measured at the loading fulcrum. Geometry then determines the displacements associated with the mode I opening load, d_I, and mode II flexural load, d_{II}.

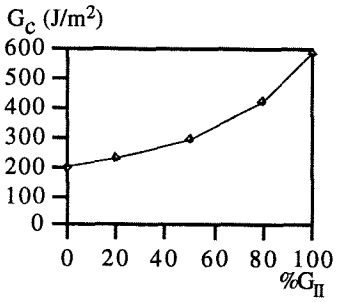

Fig. 12b Delamination toughness vs mode mixture.[35]

Care must be taken in determining the correct dis-placement value for d_{II}; it is not by itself the measured horizontal displacement of the fulcrum. Figure 13 describes a first approximation of the correct kinematic relationship to determine d_{II}. The figure shows a DCB specimen which has been loaded in a fashion which maintains a zero load contact with the rear support of the MMB rig.

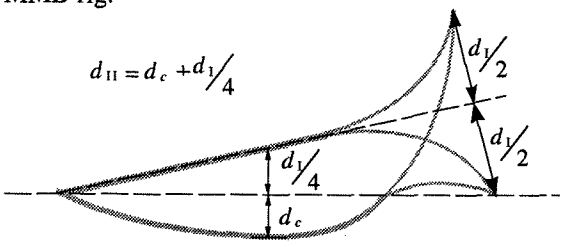

Fig. 13 Kinematics for the correct determination of d_{II}, the distance through which P_{II} acts.

This indicates that the mode II flexural load must act through an additional displacement proportional to d_I as well as the measured fulcrum displacement d_c. Figure 13 is an exaggeration for clarity, thus for small angles this additional displacement may be considered approximately $d_I/4$; thus,

$$d_{II} = d_c + \frac{d_I}{4} \tag{6}$$

For large angles, similar triangles show that $d_I/4$ should be replaced by

$$d_I \frac{L}{2}\sqrt{(2L)^2 + (d_I/2)^2} \tag{7}$$

where L is the distance from the supports to the fulcrum (see fig. 12a).

This approach is based purely on kinematics and is not completely rigorous. Giannakopoulos[39] has pointed out that a complete analysis must include deformations which might be caused by the fulcrum as it acts to bring the beam into a zero load contact with the rear support. Unfortunately this contribution would require the evaluation of a crack length dependent model for each increment of growth and negate the purely empirical evaluation of G_I and G_{II}.

The second objective relies on the application of the Irwin-Kies formulation (5) described earlier to both components of the mixed-mode superposition. Reeder and Crews[16] have worked out the equilibrium conditions for the superposed load systems shown in fig. 14.

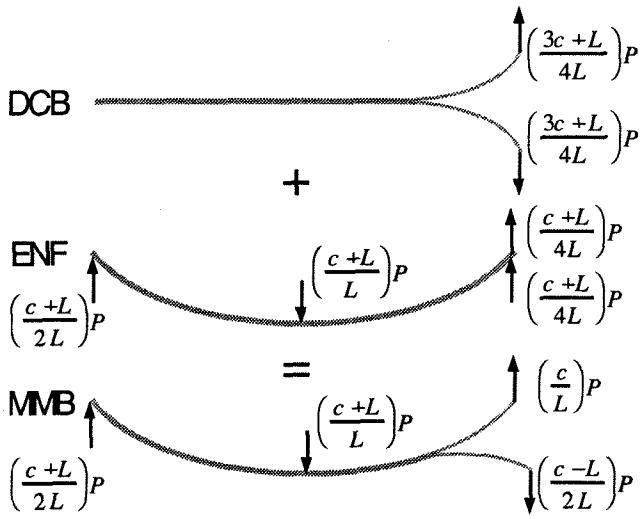

Fig. 14 Superposition of mode I and mode II components in the MMB rig.[16]

The respective mode I, P_I and mode II, P_{II} load components are proportional to the applied load P by the following equations

$$P_I = \frac{(3c-L)}{4L}P \tag{8a}$$

$$P_{II} = \frac{(c+L)}{L}P \tag{8b}$$

where c is defined in fig. 12a.

Using the compliance equation (4), the geometric relations for d_I and d_{II}, and crack growth measurements it is possible to construct compliance versus crack length curves for each load displacement pair. Curve fits are then used to determine dC/da vs a; this function is then used to complete the Irwin-Kies evaluation (eqn. 5) of G, G_I and G_{II}.

Experimental Set-Up. The data acquisition systems used in the MMB testing are identical those described for the DCB experiments. Two additional channels were necessary to record the horizontal displacement and the vertical fulcrum displacement. Two instrumented dial gauges were used to measure the displacement at those locations. The vertical displacement of the applied load point was measured by the same wheel gauge used in the DCB experiments. A photograph of the rig with the displacement gauge layout is shown in fig. 15.

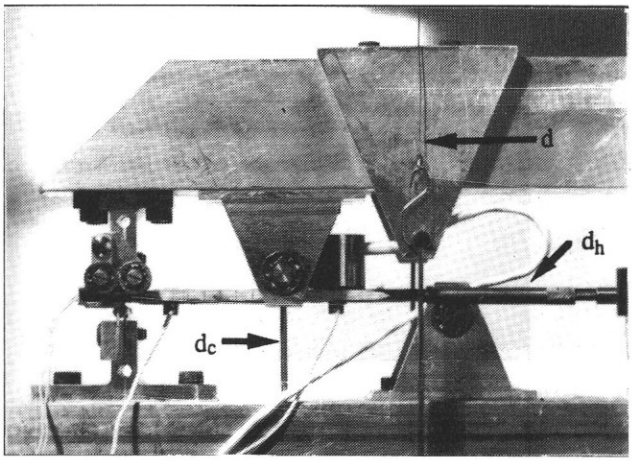

Fig. 15 Experimental set-up of MMB.

The experiments were set to achieve a balanced 1/1 mode mixture; c=41 mm was chosen based on the finite element analysis of Crews and Reeder.[16]

Data reduction and Results. A complete example of the empirical analysis is provided for one test case Figure 16a presents the load displacement curves for the three load displacement pairs. Again P_I and P_{II} are determined by equilibrium considerations and d_I and d_{II} are determined from the kinematics of the lever/ fulcrum system.

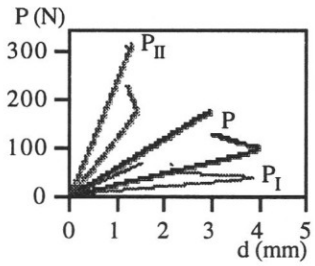

Fig. 16a Load vs displacement plots for each load/displacement pair in a MMB test, 0°/0° interface.

As a check, load displacement data for pure mode I DCB and pure mode II ENF tests are super-imposed to show that the initial and final stiffnesses are reasonable (see fig. 16b&c).

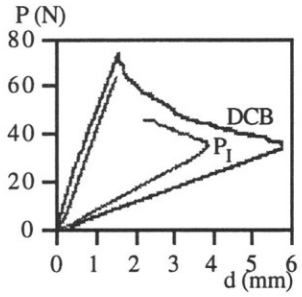

Fig. 16b Comparisson of the mode I plot to a DCB test result from ref.[37]

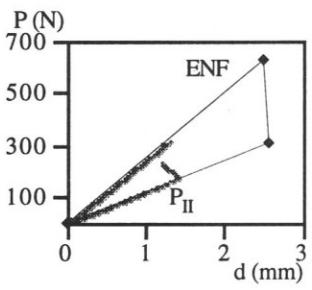

Fig. 16c Comparisson of mode II plot to an ENF test result from ref.[35]

For many of the experiments,delamination growth initiated more rapidly than expected so the crack length data exhibits some discontinuities. This is evident in the a vs d plot in fig. 17. Corresponding compliance curves and curve fits are shown in fig. 18.

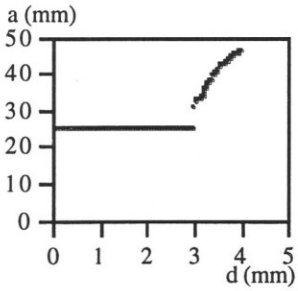

Fig. 17 Crack length vs applied displacement for a 0°/0° interface.

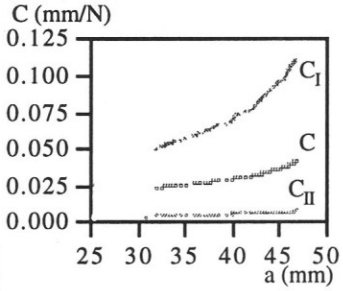

Fig. 18 Compliance vs crack-length curves for each load/ displacement pair in fig. 17.

Continuous G, G_I and G_{II} delamination toughness curves for these results are shown in fig. 19, 0°/0° interface.

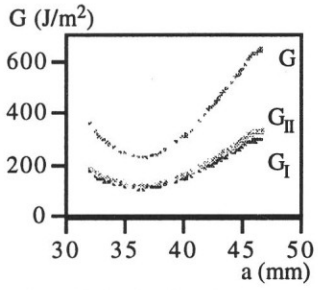

Fig. 19 Delamination toughness in terms of total G and the seperated components G_I and G_{II}.

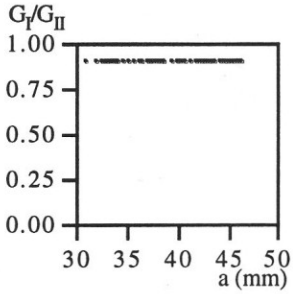

Fig. 20 Ratio of mode I to total energy release rate vs crack length.

The mode ratio is plotted in fig. 20. It is slightly less than 1.0 and nearly constant. This agrees with the FE results reported in ref.[16] Since $G = G_I + G_{II}$ a check of the calculations is readily performed in fig. 21. Mixed mode delamination toughness results for the 0°/90° interface is given in fig. 22.

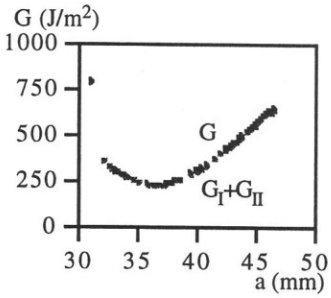

Fig. 21 Comparisson of the sum $G_I + G_{II}$ to the empirically determined total G.

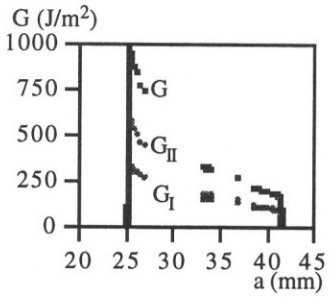

Fig. 22 Examples of delamination toughness for a 0°/90° interface.

Fractography. Bridging zones for the mixed mode tests are greatly reduced in fig.23 with respect to DCB tests.

Fig. 23 Macro-fractographs of bridging in MMB tests. a) 0°/0° interface.

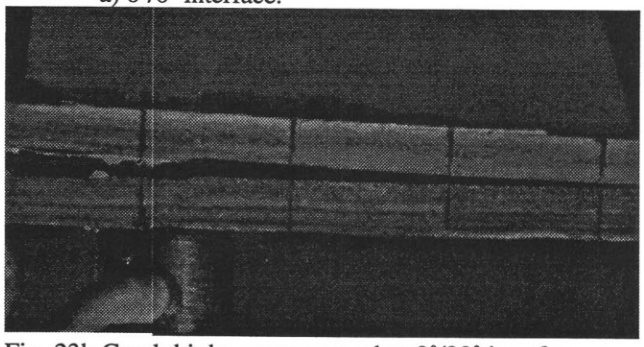

Fig. 23b Crack kinks, grows on other 0°/90° interface.

Single Edge Notch Strips

Background

The single edge notch geometry is common to polymer mechanics researchers[40] however the boundary conditions applied are usually load or stress controlled. This is true also of the Arcan double notch[41] and its single notched variation[42] used in testing fiber composites. The single edge notched strip (see fig. 2) introduced here is subjected to displacement control testing in an effort to simulate the infinite strip problems addressed by Rice[20] and Nilsson[21].

As in [41,42] the specimens are bonded to metal pull tabs, however the steel pull tabs in this case are clamped in wedge grips instead of pin loaded. Thesken and Béguelin[18] demonstrated the approach using a twin screw tensile machine and more recently Thesken[19] has tested the strip specimen in servo-hydraulic systems under extensometer control. Growth instability is a prevalent characteristic of such rigidly extended strips which makes this a useful test of dynamic fracture properties. Fortunately, under fixed grip extension, strips of this nature exhibit a steady-state energy release rate over much of the intended fracture length.[21,43]

Several variations of this rigidly extended edge notch strip, illustrated in fig. 24, shall be considered in the program. The 45° angled strip is meant to provide a balanced mixed mode specimen. The rigid double cantilever strip is meant to provide mode I loading similar to the DCB specimen but for thicker laminates.

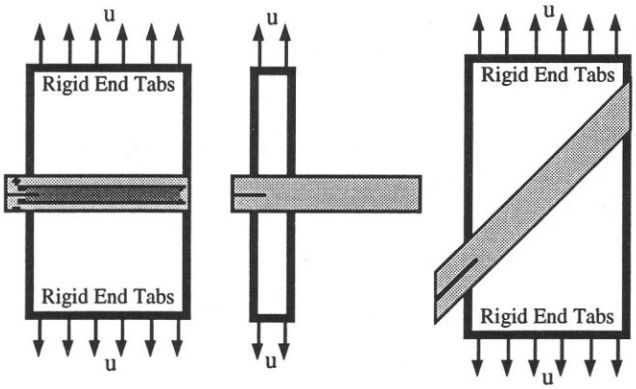

Fig. 24 Three variations of rigidly extended single edge notch (SEN) strips.

Mode I SEN strips

Material Test Matrix. During the development of the test method in [19], specimens with 11 mm total strip height were tested with the following lay-ups: $0°_{80}$ and $(0°_{39}/\pm 5°/0°_{39})$. Teflon™ starter cracks were embedded between ply 40 and 41. A second specimen group includes 0°/5° and 0°/90° interfaces as in the delamination beams but testing has not yet begun.

Specimen Preparation. The dimensions of the steel plate pull tabs were limited by the hydraulic wedge gripping system of the servo-hydraulic test machine. The thickness and width of the plates could not be greater than 20 mm and 60 mm respectively. Each plate was about 100 mm in length so that when bonded to the composite strip the overall height of the specimen was 211 mm. About 100 mm of this height are required for proper gripping leaving ample room for extensometers and other instrumentation.

The final length of each strip depends upon the desired initial crack length. Specimens containing extremely short cracks in the projected load path of the steel plates were required to be longer than the steel plates. This additional length is needed so that the graphite crack gauge can be positioned with the starter crack lying within the linear region of the gauge. Final strip lengths, 60 to 65 mm, were cut to obtain a range of initial crack lengths from 0.5 mm to 10.0 mm in length. FM 300K structural adhesive from American

Cyanamid Company was used to bond the steel tabs to the composite strips. A bonding jig maintained alignment of the specimen components during curing.

Experimental set-up. These experiments were performed using a stiff servo-hydraulic load frame rated for a 200 kN capacity. A 50 kN load cell was used to get the sensitivity necessary for the expected 10 to 30 kN load range. A pair of extensometers was placed on each end of the specimen to monitor the applied displacement field. The tests were conducted at constant displacement rate of 0.055 micron/s using a feed-back loop between one of the extensometers and the system controller. A photograph of the installed specimen is shown in fig. 25.

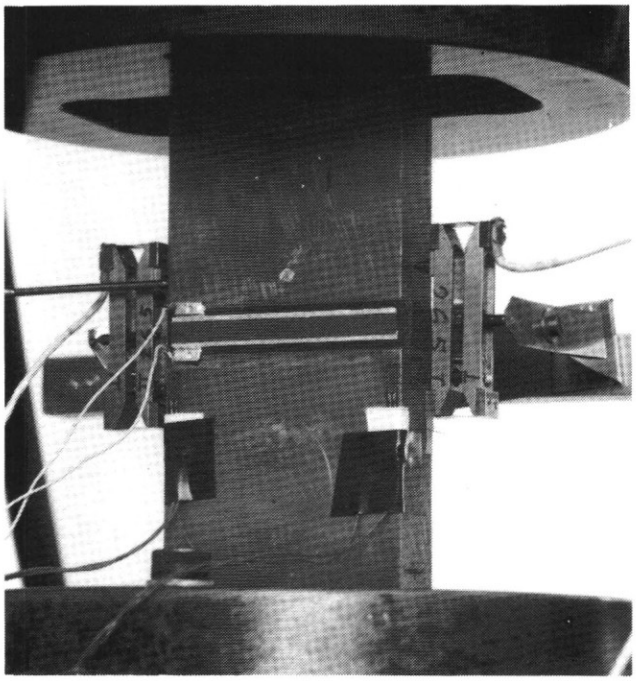

Fig. 25 Test set-up of a mode I SEN strip.

Quasi-static measurements during the fracture testing using a Macintosh PC with a Work Bench card and software. Real time graphs of the load displacement behaviour for each extensometer were also produced by an x-y chart recorder.

Reliable acquisition of the transient data from the graphite crack gauge was made with a Phillips 60 MHz digital oscilloscope. After each test the transient data was dumped to the Macintosh for storage and processing. Practice dynamic growth experiments were made on PMMA plates evaluate the transient function of the gauge. The measured growth rates for these tests, 100 to 700 m/s, compared well with PMMA data in the literature.[43]

After each composite strip, experiment maximum failure loads and displacements were noted from the system controller. Measurements were recorded of the position of the starter crack tip with respect to the graphite crack gauge and the steel plates. Fracture surfaces were then carefully sectioned from the steel plates and stored for further fractographic examinations. The steel tabs were then cleaned and reused.

Data Reduction. A typical oscillograph is shown in fig. 26. The initial voltage level V corresponds to the starter notch length in the graphite film. Together with the battery voltage V_b and eqn. (3), the data is then calibrated to crack length versus time. Piece wise continuous polynomial curve fits were then made. Delamination velocity curves are then the time derivatives of these functions.

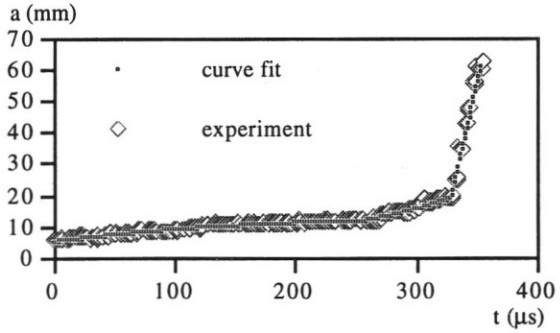

Fig. 26 Calibrated crack length vs time curve for a dynamic delamination with a polynomial curve fit.

Figure 27 presents a few of the valid time histories acquired during these tests. Analysis of the experiments was made using 2-d static and dynamic finite element methods[19]; the results are reviewed in a later section.

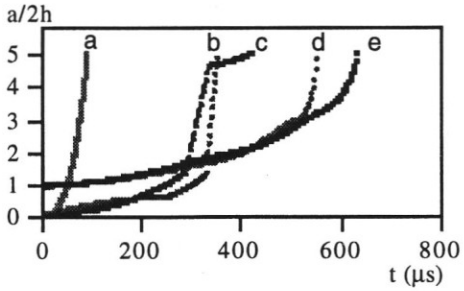

Fig. 27 Five curve fits of dynamic delamination histories: a,c&d 0°/0° interface, b&e ±5° interface.

Buckling Induced Delamination Plates

Background

Buckling induced delamination growth is an important mechanism by which the performance of laminated structures is degraded. Therefore it is natural that this type of structural element provides an important test of the transferability of delamination toughness data. The fundamental complexity of this problem has been treated in detail by numerous authors. Overviews of the

subject may be found in Storåkers[44] and Hutchinson and Suo[8]. Despite the extensive work in this area few studies are available which examine growth as well as initiation. Nilsson et al[22] have introduced theoretical and experimental methods for addressing buckling induced growth. A continuation of this work is planned for heterogeneous interfaces using the experimental methods reviewed here.

Test Methods and Results

Lay-up. A cross-ply lay-up $(90°/0°/90°)_{16}$ was used in [22] where an artificial flaw was placed beneath the first sublaminate layer. The dimensions are such that the first sublaminate behaves as a buckled thin film on an elastic substrate. The two 90° plies establish maximum stiffness in the direction transverse to the compressive loading. The anticipated local crack front lies normal to the 90° fiber directions so that kinking is restricted. This is a homogenous 0°/0° interface; modifications of this type of lay-up are planned so that 0°/5° and 0°/90° will be examined.

The laminates tested thus far were manufactured with a series of 20 mm diameter circular films placed beneath the first sublaminate layer, about 0.38 beneath the surface. Nominal plate thickness was 6.48 mm. Double Teflon™ films, 0.025 mm each, were used at each location to assure the separation of the thin layer from the substrate. Specimens were then sectioned and strain gauged according to the diagram in figure 28.

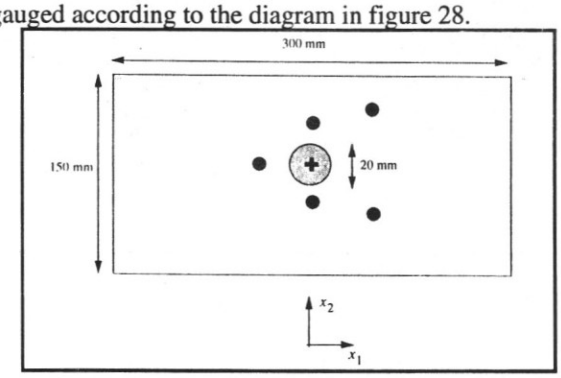

Fig. 28 Specimen geometry for plate and strain gauge layout. Dots represent gauges on the front face (thin film side) and crosses represent the gauge on the back face.[22]

The specimen geometry meets several criteria and fits into an existing anti-buckling frame which preserves the global stability of the plate. The frame supports the edges of the plate while leaving and 80 mm square window over the center of the plate. The thin film criteria allows that bulk of the plate to be modelled as an elastic substrate but requires that the film height should be at most 0.1 of the nominal plate thickness. This ratio is about 0.06 in this case. Also the flaw diameter (=20 mm) is small relative to plate width (=150 mm) to satisfy the simplifying assumption that the buckle lies within an infinite elastic sheet. These dimensions prevent global buckling within the plate, and allow local buckling of the film to occur at reasonable load levels (50 kN).

Experimental Set-up. Uniform strain may be experimentally difficult to achieve during uniaxial in-plane compressive loading of polymer composites. The strain gauges in fig. 28 were used to monitor the magnitude of these variations.

A 1000 kN servo-hydraulic load frame was used in these experiments. Figure 29a&b show an open view of the load frame and the final test configuration. The instrumented dial gauge in fig. 29b was used to measure the central out of plane displacement. Loads, central out-of-plane displacement, and the six strain measurements were all recorded on a Macintosh with WorkBench™ software.

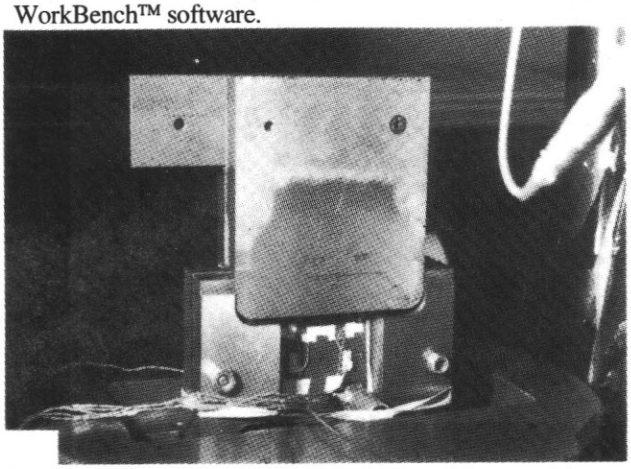

Fig. 29 BID experimental set-up. a) Load frame with acoustic emission transducer in lower corner.

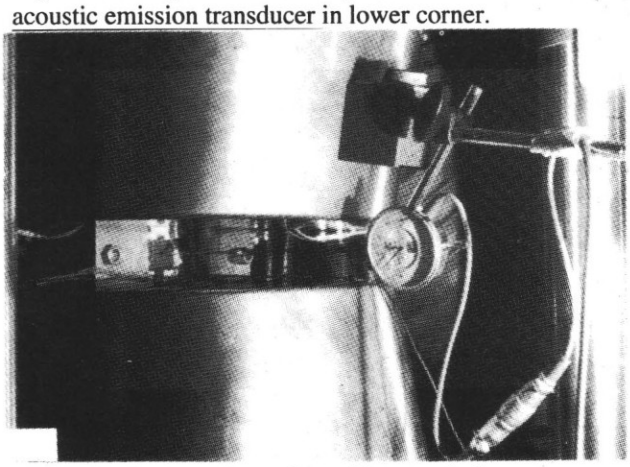

Fig. 29b Final configuration with out-of-plane displacment transducer.[22]

Acoustic emission was used as a means to follow delamination growth. A Bruel & Kjaer Acoustic Emission Pulse Analyzer Type 4429 with a 200 kHz resonant type 8313 AE transducer was used. The unit was employed using the cumulative weight mode,[45] which was found to give a clear indication of a growth event. Basically this is a simple method to approximate

the area under the amplitude versus time signal from the AE sensor response. The pulse analyzer presents this data in terms of a dimensionless number or "count". Plotting the cumulative count versus load on an x-y recorder showed that the count level was nearly unchanging during loading except when a sharp increase indicated that growth had occurred. After each growth indication the specimen was removed from the framed and examined with ultrasonic C-scan to determine the extent of delamination growth. For some cases, radiography was used as an alternative means to inspect for growth.

Results. Table 1 gives a summary of the data for case A in ref. [22]. The compressive strain ε_1 and transverse strain ε_2 are nominal values. The deviation from the average compressive strain did not exceed 4%. Using the measured loading, ε_1 and ε_2, estimates of the effective module and effective Poison's ration are also given in table 1. The central out of plane displacement, u_3 and the measured crack extensions for each side of the flaw are also listed.

Load case	ε_1 (10^{-3})	ε_2 (10^{-3})	E_1 (GPa)	ν_{12}	u_3 (mm)	Δa_U (mm)	Δa_L (mm)
A-1	2.3	0.11	50.7	0.05	0.16	0.0	0.0
A-2*	2.2	0.08	50.6	0.04	0.0	-	-
A-2	3.3	0.14	48.9	0.04	0.32	1.5	0.5
A-3	3.4	0.13	49.2	0.04	0.40	2.0	1.2
A-4	3.7	0.15	48.8	0.04	0.46	3.0	2.2
A-5	3.7	0.18	48.5	0.05	0.49	3.2	2.5
A-6	4.1	0.20	48.8	0.05	0.42	5.4	5.7

* Buckling bifurcation

Table 1. Data summary of plate A.[22]

The crack extension measurements were made from the set of C-scan maps in fig. 30.
Further discussion of these results will be given in the following analysis and discussion section.

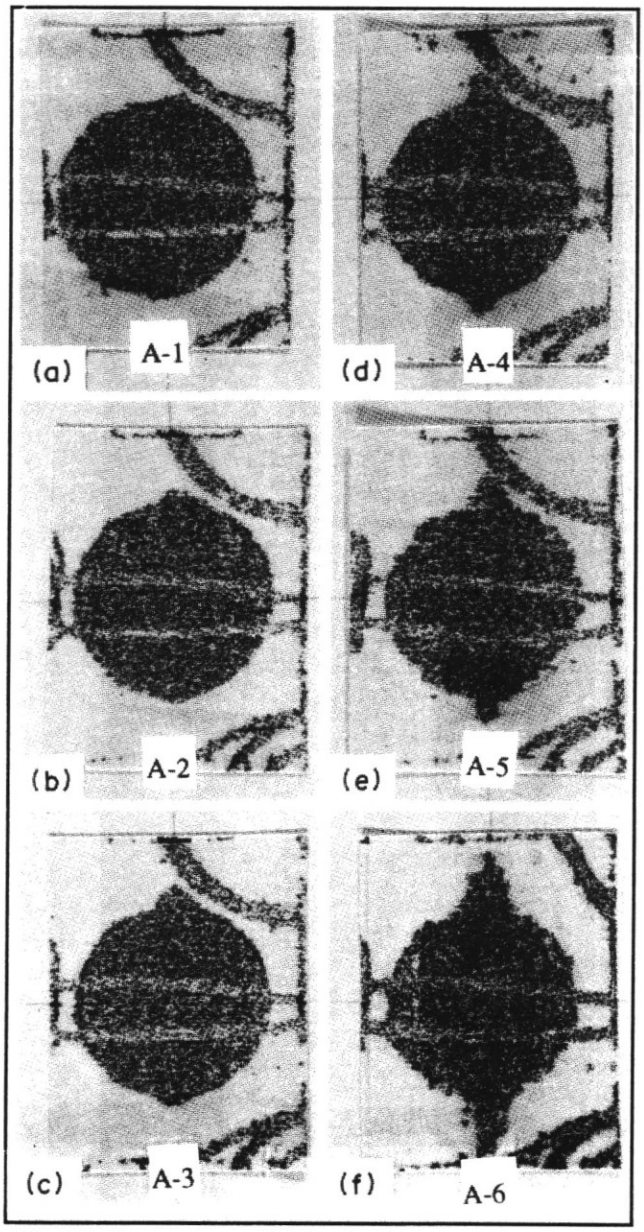

Fig. 30 C-scan maps of delamination shape for six load cases.[22]

Analysis and Discussion

The previous sections reviewed a program of experiments being used to evaluate the validity of fracture mechanics for heterogeneous interfaces. For the stable growth cases of the delamination beam specimens it was possible to evaluate directly the energy release rate from the experimental data using the Irwin-Kies formulation eqn. (5). Unstable growth during the single edge notch strip experiments makes such empirical evaluations of the data impossible. The Irwin-Kies relation is also difficult to apply the buckling induced delamination data because the compliance changes are to small to measure. Delamination criticality must be determined by other means for these cases. It was also suggested in the introduction that the sandwich specimen might be treated as a homogenous body when evaluating such fracture parameters. These and other questions are addressed using various finite element methods.

A critical evaluation of the experimental data is underway however the progress with each analysis is at various levels of completion. Sufficient results are available from the mode I DCB and SEN strip experiments so that some comparisons are possible. The following is a few examples of types of analysis being made and a discussion of the current results.

Sandwich Coupon Specimens

Heterogeneous Interface Effects. The engineering practice of fracture mechanics for delamination in composites would be simplified if the local influence of

heterogeneous interfaces could be adequately described by a global calculation of G. This is a particularly true for the analysis of the sandwich test geometries if G could determined using the solution of the homogenous body and two dimensional plane mechanics or simpler theories.

Investigations of this premiss for requires three dimensional elasto-static analysis. The main computational tool used in this effort is a self adaptive p-version of the finite element method formulated in the code STRIPE.[31,32] The code is equipped with advanced extraction methods to compute edge and vertex stress intensity factors for three dimensional cracked bodies. These methods fully generalized to evaluate the energy release rate and complex stress intensity factors for bimaterial interface cracks.

Two studies are presented here to show the influence of interface on the local energy release rate. Displacement boundary conditions are applied in both cases. The first is an evaluation of the ±5° interface used in the edge notch strip specimens. Figure. 31a shows the local G distribution through the specimen thickness for both 0°/0° and ±5° interface conditions. A similar analysis has been made for the 0°/5° interface in a DCB configuration. The extraction method breaks down for perfect 0°/angle type interfaces so an approximate result is obtained by modelling an angle/5° interface where the angle is set to the values: -1°,-0.5°, -0.1°, approaching zero. Thus the first analysis is for a ($0°_{11}$/angle/±5°/$0°_{8}$/±5°) lay-up and does not correspond precisely to the experimental configuration. Figure 31b compares the total energy release rate for the three angle/5° interfaces to the 0°/0° interface.

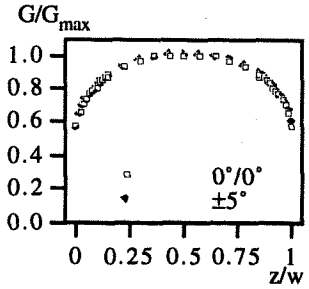

Fig. 31a SEN strip.

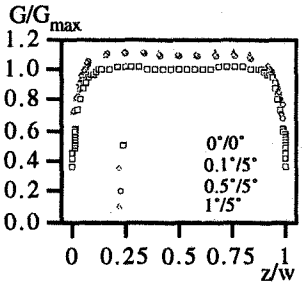

Fig. 31b DCB strip.

Fig. 31 3-d finite element solutions of the through thickness G distributions. Values are normalized with respect to central G value of the 0°/0° solution for each geometry.

A comparison of figs. 31a&b indicates that the heterogeneous interface has a stronger effect on the local G distribution in the DCB specimen than in the edge notch strip specimen. The G distribution for the ±5° interface in the edge notch strip is nearly indistinguish-able from the corresponding homogeneous interface. Although the interfaces and loading are not exactly the same in each specimen, the characteristic dimensions of the two sandwich lay-ups may actually offer the best explanation for the difference. The fraction of the off-axis interface plies in the strip specimen is about four times smaller than the fraction in the DCB specimen. Further more the presence of the two ±5° plies on the outer skin of one arm of the DCB must also play a role in altering the local G distribution.

Looking further at the DCB results in fig. 31b it is seen that the small perturbations of the interface angle is insignificant to the general effect of the interface. Clearly other aspects of this configuration must dominate the energy release rate. However this does give an indication that small manufacturing uncertainties in fiber angle need not be treated when performing such calculations.

Thickness constraint. The three dimensional interface results for the single edge notch strip suggests that interface effects should be small enough that the specimen could be evaluated as a homogeneous body using 2-d finite element methods. This is not the case for the DCB specimen which is undergoing further study. However another question is raised when looking at figs. 31a&b.

The through thickness distribution of G in the DCB specimen is nearly constant over most the width where it continuously varies through the strip. This three dimensional effect through the width of the specimen is expected due to the large height to width ratio; about 1/2 for the edge notch strip and about 1/6 for the DCB.

This effect is studied further in comparison of 3-d FE solutions to 2-d plane FE solutions for different crack lengths. The results are have been normalized with respect to Rice's[18] solution for an plane strain infinite strip and plotted in fig. 32. The max and min value of the through thickness G distributions are presented along with the average through thickness value. For the cases presented the average solution varied from 0.88 to 0.92 of the maximum G. The overall behaviour of the curve is familiar for this type of specimen geometry (see Carlsson et al[43]) where G rises to some nearly constant "steadt-state" fraction of G_{∞}. The plane strain and plane stress solutions appear as upper and lower limits to the 3-d average value.

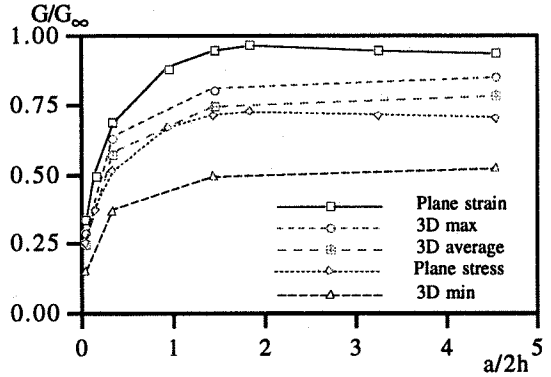

Fig. 32 Comparisson of static G/G_∞ solutions vs normalized crack length. G_∞ is the plane strain solution for an infinite strip. $2h$ is the total height of the composite strip. G_{max}, G_{ave} and G_{min} are the max, through thickness average and min values from a 3-d solution at each crack length. Plane strain and plane stress values are from 2-d finite element solutions.

Critical Energy Release Rates G_{IC}. Initiation values for mode I crack growth in the strip specimen were evaluated using a 2-d plane strain FE model. The results are summarized in fig. 33a with respect to initial crack length. The values do not appear to be independent of crack length but the data are too few to draw firm conclusions. Except at a=0.5 mm the ±5° interface has lower initiation values. Figure 32b summarizes the results for the empirical evaluations of the DCB data. For all cases, the DCB data are greater than the SEN results.

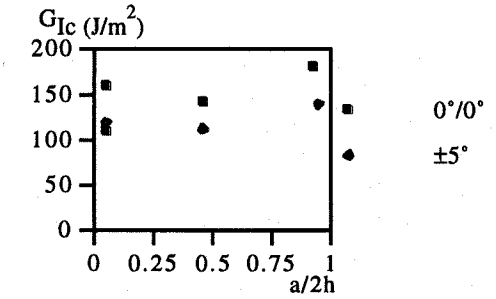

Fig. 33a SEN G_{Ic} values from 2-d plane strain solutions vs initial starter crack length.

Delamination Criticality and Growth Rates. The unstable dynamic delamination data for the SEN strips (see fig. 27) was used as input to the 2-d elasto-dynamic finite element code DYNCRACK[33]. The code incorporates a convecting G-integral in a zone of convecting crack tip elements as shown in fig. 34. The program has been adapted to model symmetry planes of orthotropic materials and has tested accurately against closed form solutions for an orthotropic strip.[18] The static 2-d FE solutions of the previous section were used as initial conditions and the displacement boundary

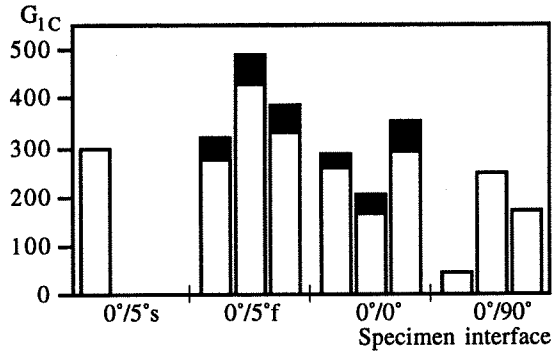

Fig. 33b DCB G_{Ic} values. The drop between upper and lower critical points, defined in fig. 8c, appears as solid black.

condition on the steel tabs is assumed constant during the entire growth event. The dynamic G histories reviewed here were generated in ref.[19], further details of the analysis can be found there.

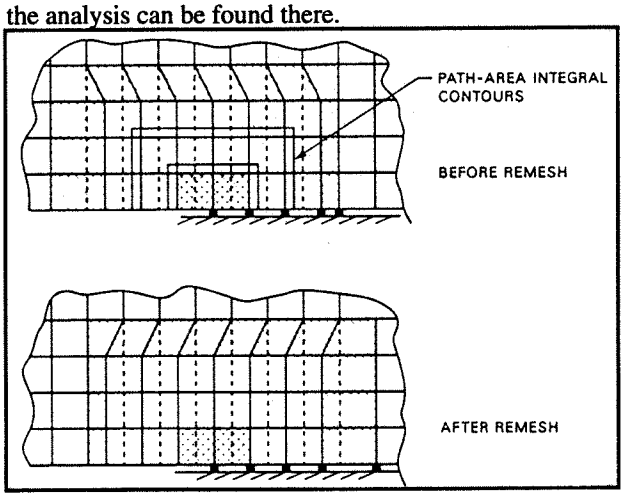

Fig. 34 Moving crack tip element zone with embedded G-integral.[33]

Figure 35 presents a comparison of five cases: three for 0°/0° interfaces and two for ±5° interfaces.

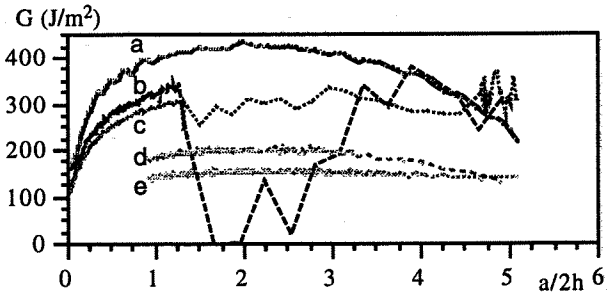

Fig. 35. Dynamic energy release rates vs normalized crack length for the five delamination histories in fig. 27; a,c&d 0°/0°and b&e ±5°. $2h$ is the total strip height.

Two of the specimens presented had 10 mm starter cracks. The others had 0.5 mm starter cracks. Unfortunately crack velocity data was not successfully recorded for the 5 mm SEN specimens shown in fig. 35.

Note that there is no clear difference between the 0°/0° and the ±5° results.

Figure 36 presents two examples of G vs $\dot{a}/Cr$ curves for a_o=0.5 and a_o=10 mm. Cr is the surface wave speed for this orthotropic plane; it is about 1788 m/s.[19] Although the initiation values for G are about the same, the resulting velocity dependence is completely different.

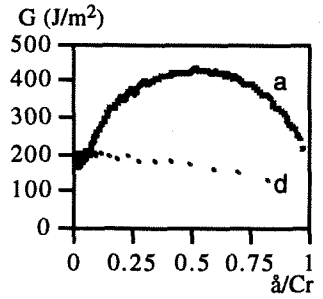

Fig. 36 Dynamic energy release rates vs normalized delamination velocity for case a. and d. Cr is the surface wave speed.

The short crack specimen must be strained to a higher internal energy before growth initiates which explains the rise in energy release rate. It is however unexpected that crack velocity would continue to increase even as G decreases. It is also interesting that the long crack specimen endures a period of slow growth before accelerating to high speed, and that this all takes place at relatively lower G values.

These data require further study but an attempt to draw some general conclusion has been made. Returning to fig. 35 it is seen that the short crack specimen data all rises with crack growth towards the "steady state" plateau observed in the static analysis in fig. 32. The long crack data appear nearly constant at the start since the crack already lies in the steady-state area. A rank A through E can be assigned to each specimen result based upon an estimate of the G value in the steady state region. The corresponding average crack speed for each specimen estimate is then plotted in fig. 37.

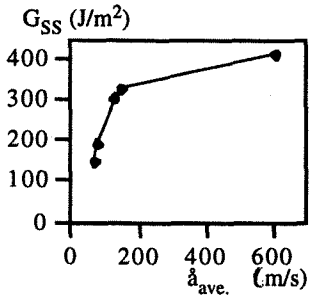

Fig. 37 G_{SS} vs average crack speed. G_{SS} is an estimate of G in the "steady-state" range of the strip beginning about $a/2h \approx 12.5$

Figure 37 shows a trend of increasing crack speed with G similar to other dynamic fracture data.

Trends in DCB growth rates have also been examined; the measured stable delamination growth rates are summarized in fig. 38. Speeds range from 0.05 to 0.15 mm/s. The highest speeds were recorded for the 0°/0° interface and the slowest for the 0°/90° interface. For all cases crack growth began fast and then slowed, except where the Teflon™ spray was used to make the starter crack. Initiation of growth from the Teflon™ spray was slow but then became faster. Apparently the extremely sharp starter crack makes it difficult to build up excessive strain energy in the specimen. Looking at the delamination resistance curves in fig. 9 it is seen that the slowing crack speed trend seems consistent with increasing energy release rates and results reported by Daniel and co-workers[26,27]. However, further experiments and analysis are needed to draw conclusions regarding G vs $\dot{a}$.

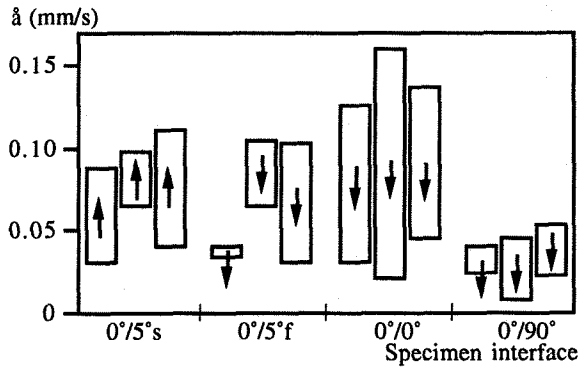

Fig. 38 Trends in delamination rates for DCB tests. Arrows indicate increasing or decreasing rates.

Composite Structural Element

Buckling induced Delamination. The experimental and analysis program of sandwich coupons is meant to provide a data base to predict initiation and growth of damage in representative structural elements. The two types of specimen geometries studied exhibit a range of growth behaviour from stable to unstable/dynamic propagation. The experiments thus far completed with BID plates has focused on the stable growth regime; however, there is an interest in the program to design experiments which will cover the entire range of growth including catastrophic failure. The analysis of initiation and stable growth regime shall involve application of the 3-d p-version finite element code STRIPE[31,32] and the plate/shell delamination algorithm described in ref.[22,34] It is known that fracture surfaces may come into contact during buckling induced delamination; the plate/shell algorithm[22,34] is equipped to handle contact and STRIPE is presently being enhanced with new contact procedures.

The results of BID experiments reviewed above for the case of a 0°/0° interface were analyzed using the later

plate/shell finite element method.[22] The predicted buckling strain 0.212 % from computations agreed well with experiment 0.215%. Figure 39 also shows a good agreement between the measured out-of-plane displacement and the finite element solution.

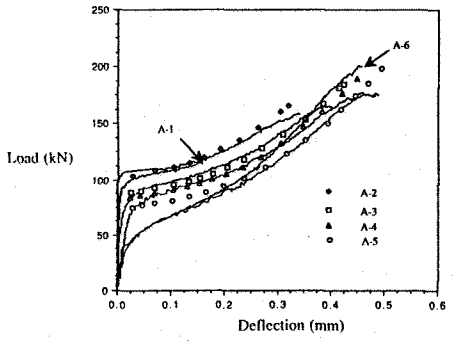

Fig. 39 Compressive load vs central out-of-plane displacement for load cases A-1 to A-6. Experimental results are solid lines, numerical results are symbols.[22]

Crack growth initiated at 0.33% strain in the experiments which corresponds to a G_c=217 J/m^2 in the computational analysis. This value is reasonable with respect to the mixed-mode results reported by Ljung[35] in fig. 12b. Assuming a constant delamination growth resistance this value was used to predict the subsequent growth cases. Successive delamination fronts from computations are shown in fig. 40. Applied strain versus crack growth results are compared to the experimental results in fig. 41.

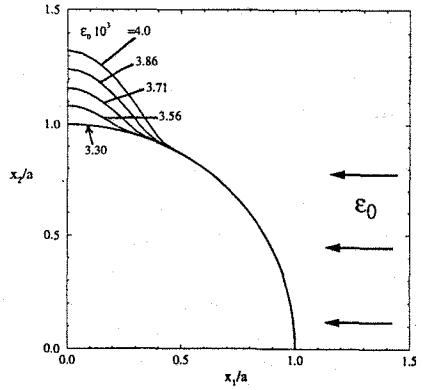

Fig. 40 Succesive delamination fronts vs compressive strain.

Figure 41 shows that growth predictions agree extremely well with the experimental data. Although this result is encouraging and further experiments are planned to examine the influence of test parameters. These include flaw shape, size and thickness, flaw depth, and interface character. The interface character is a

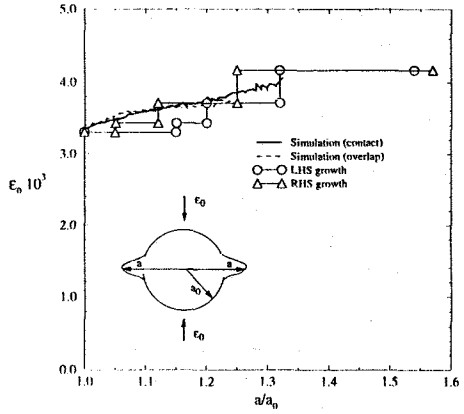

Fig. 41 Nominal strain vs delamination growth. Numerical simulation and results for plate A.[22]

description of the angles of the adjacent interface plies relative to the crack front. The delamination growth and acoustic emission measurement techniques need to be improved to meet the objectives of the program. Future experiments shall examine shadow Moiré as a means to infer growth rate to the embedded delamination. Contours of the buckled shape should also give an extra check on the accuracy of analysis. Improvements of the acoustic emission monitoring shall be made by using a multiple channel system capable of greater sensitivity and spatial location of scources. It is hoped that smaller increments of growth can be detected for correlation with growth rate. A few tests should be planned which exhibit growth instability and catastrophic failure.

Conclusions

A program to determine the relationship between delamination criticality, crack length, growth rate and acoustic emission for heterogeneous interfaces was reviewed. Progress of the experimental and theoretical investigations of delamination growth was presented; details and results of the acoustic emission studies will be presented in a companion paper.[2]

Sandwich coupon specimens were introduced as a means to characterize interface effects in delamination growth. Three dimensional finite element results demonstrates in one case, a ±5° interface being a 1/40 fraction of the sandwich, that such specimens might be analyzed as homogenous bodies. These results likely depend on the fraction of interface plies and their angle relative to the bulk laminate so a parametric study shall continue. There is an interest to establish under what conditions the homogenous body solution is no longer a good approximation of the interface solution.

Methods for the application of a graphite crack gauge to delamination measurements in carbon composites were reviewed. The crack gauge measurements for DCB tests were shown to compare well to travelling microscope and radiographic measurements. The gauge has been used successfully to

measure a range of crack speeds from $5 \cdot 10^{-5}$ m/s to 2000 m/s.

The use of the crack gauge enabled the application of the Irwin-Kies relation to determine continuous delamination resistance curves. This approach was extended to analysis of fully instrumented Mixed Mode Bending tests. Mode separation of the global mode mixture was achieved based upon empirical determination of the mode I and mode II load/displacement pairs and the Irwin-Kies relation. It should be mentioned the empirically determined mode ratios are in reasonable agreement with those computed by Crews and Reeder for the same rig parameters.

A macro-ccd camera was used to follow delamination growth in both DCB and MMB tests. The amount of bridging for each interface in the DCB test was distinctly different. Although the amount of bridging fibers for the 0°/5° interface was less than in the 0°/0° interface, there was no clear difference in the delamination growth resistance data for these two interfaces. The 0°/90° interface developed intralaminar fracture with substantial bridging parallel to the crack front. Accordingly, the 0°/90° interface under mode I loading develops the highest, monotonic increasing delamination growth resistance.

The presence of a mode II loading component in the MMB test completely changes these observations. Although results for the 0°/5° interface were not shown, fiber bridging was substantially reduced for this and the other interfaces. Most interesting was the change observed for the 0°/90° interface. There the delamination kinked across the 90° ply to the upper interface and remained trapped in the interface through out the experiment. The only fiber bridging observed was a bundle of fibers at the kink and delamination growth resistance decreased with crack growth. Fot the 0°/0° interface, mixed-mode delamination growth resistance decreased through the initial growth and then increased at the end.

A single edge notch strip was used as alternative delamination toughness specimen capable of producing dynamic toughness data. The specimen is analogous to the infinite strip problem and therefore has a steady state region where G is independent of crack length. Static 2-d and 3-d solutions of G were made for different crack lengths. These showed how thickness constraint effects scale the steady state value of G.

G_{Ic} values were computed for the SEN strips using 2-d plane strain finite elements and compared to empirical results for the DCB tests. In general DCB G_{Ic} values were greater than SEN G_{Ic} for all cases. This trend was already observed between SEN and DCB test data for AS4/3506-1[18] and requires further investigation. Opposite trends are observed between the low angle, 0°/5 or ±5° interfaces, and their respective 0°/0° counterparts for each specimen. The low angle interface G_{Ic} values would be expected to be larger due to a larger resin pocket at the starter crack. This is seen in the DCB results but the opposite is found in the SEN values. Further experiments are needed to verify this trend and to determine an explantion.

Dynamic delamination histories were reported for five of the SEN tests. These have been analyzed using the dynamic finite element code DYNCRACK with moving crack tip elements. For many cases relatively slow crack growth preceded a marked jump in crack speed. This transition is no doubt material related but it is uncertain whether it is do to random quality variations or a verifiable damage evolution behaviour. The continuous delamination toughness vs growth rate behaviour is difficult to interpret. However, by ranking the dynamic toughness data according to estimates of the "steady-state" G_{ss} value and plotting them against average crack speed, an increasing function of crack speed is observed.

Growth rates are observed to decrease with increasing delamination toughness in the DCB tests. This is consistent with the increasing size of the bridging zone which was seen in the video recordings of the tests. The data for the Teflon™ spray starter cracks is incomplete but it appears that these cracks initiate at lower growth rates then accelerate.

Experimental and analytical methods for the analysis of buckling induced delamination growth were reviewed with an example. The test results agree well with numerical simulations for the highly specialized configuration. The delamination growth in this BID test began from double Teflon™ films and extended no more than 6 mm. Microscopic observations showed no evidence of damage in the plies adjacent the crack plane nor fiber bridging. Comparison to coupon data reported here should only be made over similar size scales ahead of the starter cracks. This is where many of the DCB results for homogenous interfaces show upper and lower critical G_{Ic} values followed by some length of constant toughness. Thus this is an example suitable for linear elastic fracture mechanics. The role of interface, growth rate, flaw depth and geometry, starter crack sharpness, fiber bridging, residual stresses etc are likely to introduce non-linear material effects already observed in the above 2-d coupon tests. Therefore, improved BID experiments with varied parameters are planned to more rigorously asses the transferability of criticality, growth rate and acoustic emission activity data.

Acknowledgements. The work presented here, has been partially funded by the Swedish Defence Materiel Administration and conducted under the guidance of Dr. P. Sindelar.

References

(1) Aoki, R.M. (1993) GARTUER: Proposal for the formation of an Action Group, "Damage Propagation in Composite Structural Elements," DLR-Institute of Structures and Design, March 1993, Stuttgart.

(2) Thesken, J. C. and Henriksson, A. (1994) "Acoustic emission as a predictor of delamination growth rate and criticality," The Aeronautical Research Institute of Sweden, FFA TN 1994-xx, also *Proc. 19th ICAS, Sept 18-23, Anaheim.* (in preparation)

(3) Friedrich, K., ed. (1989) "Applications of Fracture Mechanics to Composite Materials." Elsevier, New York.

(4) O'Brien, T.K. (1990) "Towards a damage tolerance philosophy for composite materials and structures, " Composite Materials: Testing and Design (Ninth Volume), ASTM STP 1059, 7-33.

(5) Olsson, R. (1991) " Factors influencing the interlaminar fracture toughness and its evaluation in composites," The Aeronautical Research Institute of Sweden FFA TN 1991-34.

(6) Johnson, W. S. and Mangalgiri, P. D. (1987) "Investigations of fiber bridging in double cantilever beam specimens," J. Comp. Techn. and Research 9 (1), 10-13.

(7) Wilkins, D. J. , Eisenmann, J. R.. , Camin, R. A., Margolis, W. S. and Benson , R. A. "Characterizing Delamination Growth in Graphite-Epoxy," Damage in Composite Materials, ASTM STP 775, 168-183.

(8) Hutchinson, J. W. and Suo, Z (1991) "Mixed mode cracking in layered materials," Advances in Applied Mechanics, Vol. 29, 63-191.

(9) Z. Suo and J. W. Hutchinson (1989) "Sandwhich Test Specimens for Measuring Interface Crack Toughness", Materials Science and Engineering, A107, 135-143.

(10) Hutchinson, J. W. (1992) private communication

(11) Suo, Z., Bao, G., Fan, B. and Wang, T. C. (1990) "Orthotropy rescaling and implications for fracture in composites," Int. J. Solids Structures 28, 235-248.

(12) Z. Suo, G. Bao and B. Fan (1992) "Delamination and R-Curve Phenomena Due to Damage", J. Mech. Phys. Solids, vol 40, no 1, 1-16.

(13) G. Bao and Z. Suo (1992)" Remarks on Crack-Bridging Concepts", Applied Mechanics Review, vol 45, no 8, August, 355-366.

(14) S. Östlund and F. Nilsson (1993) "Cohesive Zone Modeling of Process Regions for Cracks in Linear Elastic Structures-Fundamental Aspects," Fatigue and Fracture of Engineering Materials and Strucutres, Vol. 16, No.2, 215-235.

(15) S. Östlund and F. Nilsson (1993) "Cohesive Zone Modeling of Damage at the Tip of Cracks in Slender Beam Structures," Fatigue and Fracture of Engineering Materials and Strucutres, Vol. 16, No. 6 pg 663-676.

(16) Crews Jr., J. H. and Reeder, J. R. (1990) "Mixed-Mode Bending method for delamination testing," AIAA Journal, Vol. 28, No. 7, 1270-1276.

(17) Crews Jr., J. H. and Reeder, J. R. (1991) "Nonlinear Analysis and Redesign of the Mixed-Mode Bending Delamination Test," NASA Technical Memorandum 102777.

(18) Thesken, J. C. and Ph. Béguelin, (1991) "Analysis of mode I dynamic delamination in a composite strip: computational and experimental methods," Proc. ICCM/VIII, SAMPE, 27-E, 1-12.

(19) Thesken, J. C. (1994) "Theoretical and experimental investigation of dynamic delamination in carbon fiber/epoxy composites," The Aeronautical Research Institute of Sweden, FFA TN 1994 (in preperation).

(20) Rice, J.R., "A path independent integral and the approximate analysis of strain concentration by notches and cracks", *Journal of Applied Mechanics,* (June 1968), pp.379-386.

(21) Nilsson, F., " Dynamic stress intensity factors for finite strip problems", *International Journal of Fracture Mechanics,* 8, (1972), pp.403-411.

(22) Nilsson, K.-F., Thesken, J. C., Sindelar, P., Giannakopoulos, A. E. and Storåkers, B. (1993) "A Theoretical and Experimental Investigation of Buckling Induced Delamination Growth," J. Mech. Phys. Solids, Vol 41, No.4, 749-782.

(23) Friedrich, K., Walter., R., Carlsson, L. A., Smiley, A. J., Gillespie Jr., J. W. (1989) "Mechanisms for rate effects on interlaminar fracture toughness of carbon/epoxy and carbon/PEEK composites," Journal of Maerials Science, 24,3387-3398.

(24) Davies, P. and Benzeggagh, M. L. (1989) "Interalmianar mode I fracture testing," Application of Fracture Mechanics to Composite Materials, Friedrich, K. ed., Elsevier, New York, 81 -112.

(25) Smiley, A. J. and Pipes, R. B. (1987) "Rate effects on mode I interlaminar fracture toughness in composite materials," J. Composite Mat. 21 (7), 670-687.

(26) Daniel, I. M., Shareef, I. and Aliyu, A. A. "Rate effects on delamination fracture toughness of graphite/epoxy,"Toughened Composites, ASTM STP 937, 260 - 271.

(27) Yaniv, G. and Daniel, I.M., "H-T DCB Specimen for study of rate effects on fracture toughness of composites", *ASTM STP 972,* (1988), PP.241-258.

(28) Achenbach, J.D. and Harris, J. G. (1979) "Acoustic emission from a brief crack propagation event," Journal of Applied Mechanics, Vol. 46, 107-112.

(29) Thesken, J. C. (1993) "Application of a graphite crack gauge for delamination measurements in carbon fiber composites," The Aeronautical Research Institute of Sweden , FFA TN 1993-26.

(30) Stalder, B., Beguelin, PH, Roulin-Moloney,A.C., and Kausch, H.H., "The graphite guage and its application to the measurement of crack velocity", *Journal of Material Science*, 24 (1989), pp.2262-2274.

(31) Andersson, B. Babuska, I. von Petersdorff, T. and Falk, U.(1992) Reliable stress and fracture mechanics analysis of complex aircraft components using a h-p version of the finite element method," The Aeronautical Institute of Sweden , FFA TN 1992-17.

(32) Andersson, B. Babuska, I. and Falk, U. (1990) "Accurate and reliable determination of edge and vertex stress intensity factors in three-dimensional elastomechanics," ICAS-90-4.9.2, Proceedings of the 17th Congress of the International Council of Aeronautical Sciences, 1730-1746.

(33) Thesken, J. C. and Gudmundson, P. (1991) " Application of a moving variable order singular element to dynamic fracture mechanics," International Journal of Fracture, 52, 47-65.

(34) Nilsson, K.-F. (1994) "Simulation of Buckling-Driven Crack Growth in Layered Materials," Proc. 19th Congress of the International Council of Aeronautical Sciences, Sept. 18-23, Anaheim.

(35) Ljung, K. (1992) "Mixed Mode Bending tests of the interlaminar fracture toughness of carbon/epoxy," The Aeronautical Research Institute of Sweden, FFA TN 1992-04.

(36) Carlsson, L.A. and Pipes, R.B. (1987) Experimental Characterization of Advanced Composite Materials, Prentice-Hall, New Jersey.

(37) Brandt, F. and Frii, I. (1993) "Experimental studies of mode I delamination along realistic interfaces," The Aeronautical Rezearch Institute of Sweden, FFA TN 1993-32.

(38) Nilsson, S. (1987) "Determination of mode I energy release rate GIc, in unidirectional carbon fiber/epoxy laminate," The Aeronautical Research Institute of Sweden, FFA TN 1987-05 (in Swedish).

(39) Giannakopoulos, A. E. (1994) private communication

(40) Kinloch, A. J. and Young, R. J. (1983) Fracture Behaviour of Polymers, Elsevier Applied Science Publishers, Essex.

(41) Arcan, M. , Hashin, Z. and Voloshin, A. (1978) "A method to produce uniform plane stress states with applications to fiber-reinforced materials," Experimental Mechanics, April 1978, 141-146.

(42) Jurf, R. A. and Pipes, R. B., (1982) "Interlaminar fracture of composites," J.Composite Materials, Vol. 16, 386-394.

(43) Carlsson,J., Dahlberg, L. and Nilsson,F.,"Experimental studies of the unstable phase of crack propagation in metals and polyners", *Proceedings of an international conference on Dynamic Crack Propagation.,* Ed. G.C. Sih, (July 1972),pp.165-181.

(44) Storåkers, B. (1989) "Nonlinear aspects of delamination in structural members," Proc. 17th International Congress of Theoretical and Applied Mechanics, (Eds Germain, P., Piau, M., and Caillerie, D.), 689-718.

(45) Carlsson, L. A. and Norrbom, B. (1983) J. Mater. Sci. 18, 2503.